Electronic Supplementary Information

Bioinspired Large-scale Production of Multidimensional High-rate Anodes for Both Liquid & Solid-state Lithium Ion Batteries

Shenghui Shen,[a] Shengzhao Zhang,[a] Shengjue Deng,[a] Guoxiang Pan,[b] Yadong Wang,[c] Qi Liu,[d] Xiuli Wang,[a] Xinhui Xia,[a,e] Jiangping Tu*[a]*

[a] *State Key Laboratory of Silicon Materials, Key Laboratory of Advanced Materials and Applications for Batteries of Zhejiang Province, and Department of Materials Science and Engineering, Zhejiang University, Hangzhou 310027, P. R. China. E-mail: helloxxh@zju.edu.cn*

[b] *Department of Materials Chemistry, Huzhou University, Huzhou, 313000, China*

[c] *School of Engineering, Nanyang Polytechnic, 569830, Singapore*

[d] *Department of Physics, City University of Hong Kong, Kowloon, 999077, Hong Kong*

[e] *Key Laboratory of Advanced Energy Materials Chemistry (Ministry of Education), College of Chemistry, Nankai University, Tianjin 300071, China*

Shenghui Shen and Shengzhao Zhang contributed equally to this work.

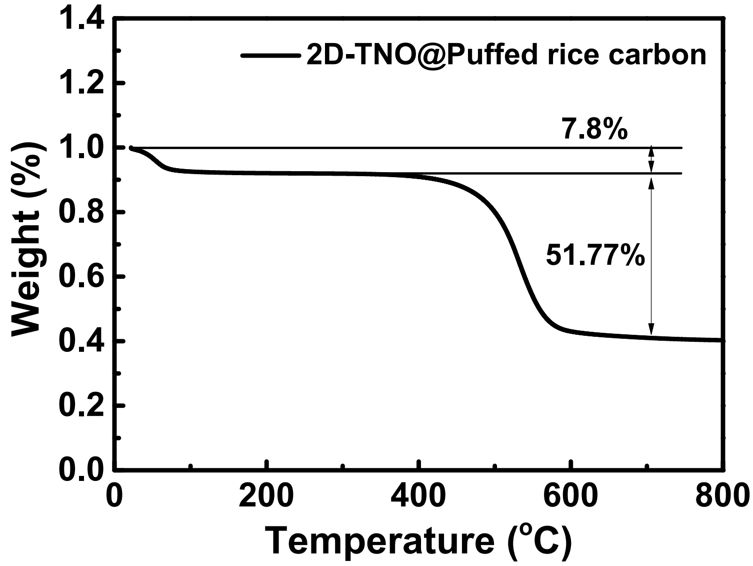

Fig. S1. TG curves of the 2-TNO@puffed rice carbon sample.

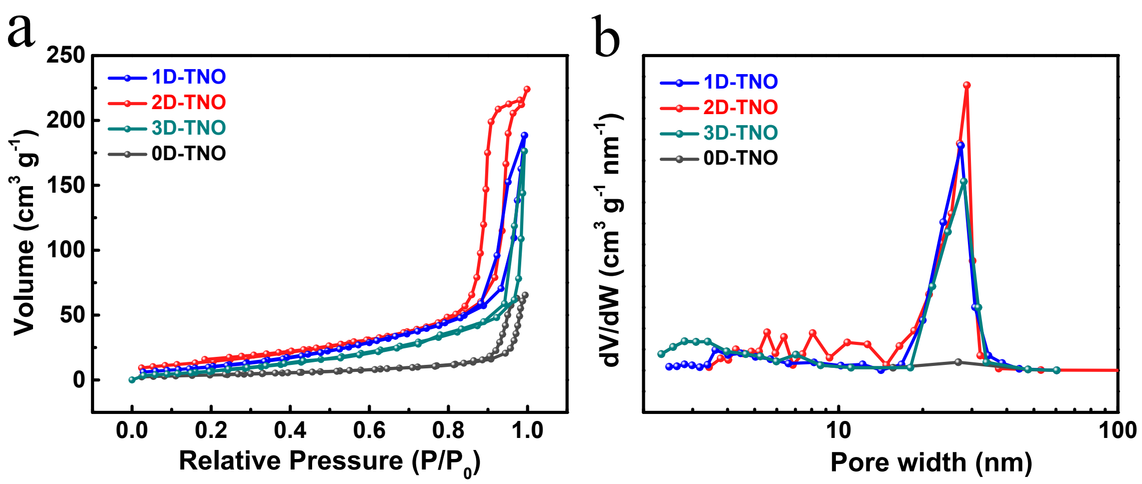

Fig. S2 (a) N_2 adsorption-desorption isothermal analysis of 0D/1D/2D/3D-TNO samples; (b) Pore size distribution of 0D/1D/2D/3D-TNO samples.

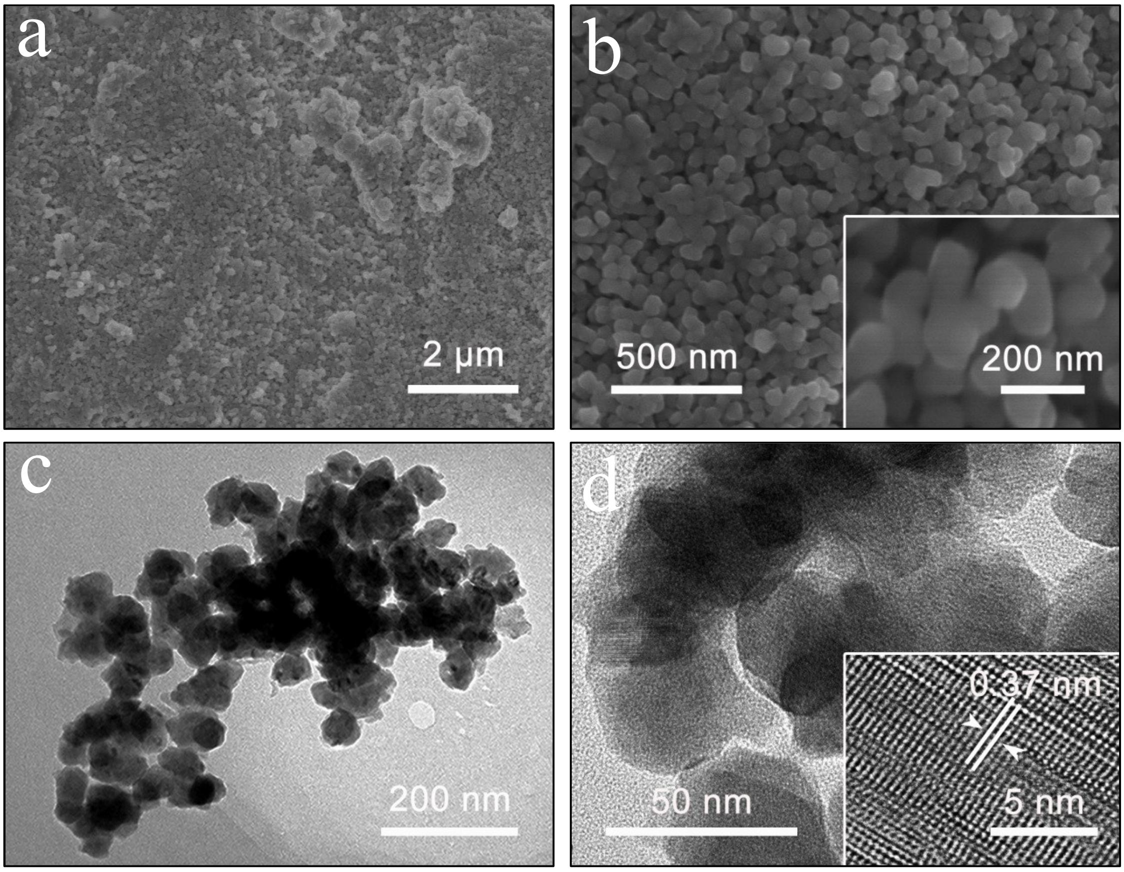

Fig. S3 SEM (a-b) and TEM-HRTEM (c-d) images of 0D-TNO sample.

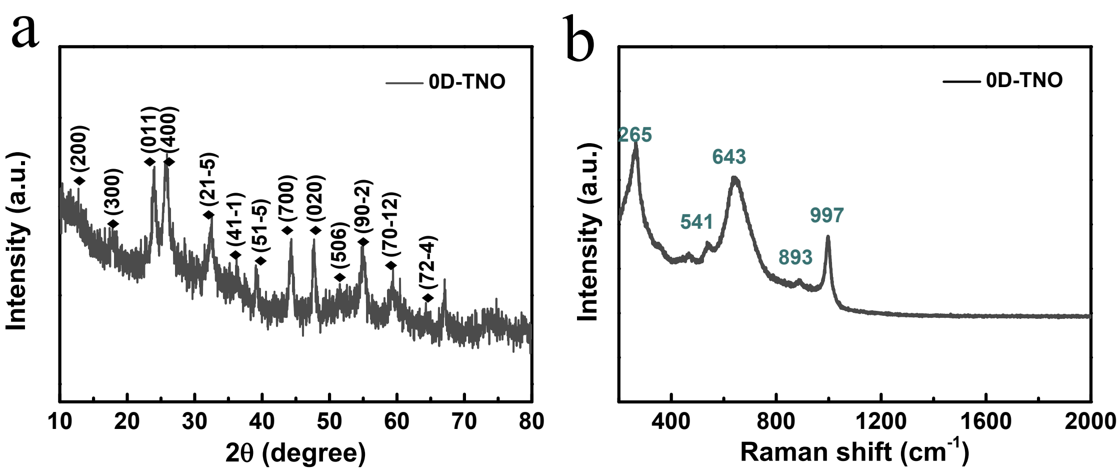

Fig. S4 XRD pattern (a) and Raman spectra (b) of 0D-TNO sample.

As shown in the XRD pattern of 0D-TNO sample (**Fig. S2a**), the sample presents the same peaks as the 1D/2D/3D-TNO samples, verifying the successful synthesis of the pure

$Ti_2Nb_{10}O_{29}$ phase without any purity. In Raman spectra (**Fig. S2b**), characteristic peaks of $Ti_2Nb_{10}O_{29}$ (265 cm^{-1}, 541 cm^{-1}, 643 cm^{-1}, 893 cm^{-1} and 997 cm^{-1}) could be detected in the sample, further confirming the successful synthesis of $Ti_2Nb_{10}O_{29}$.

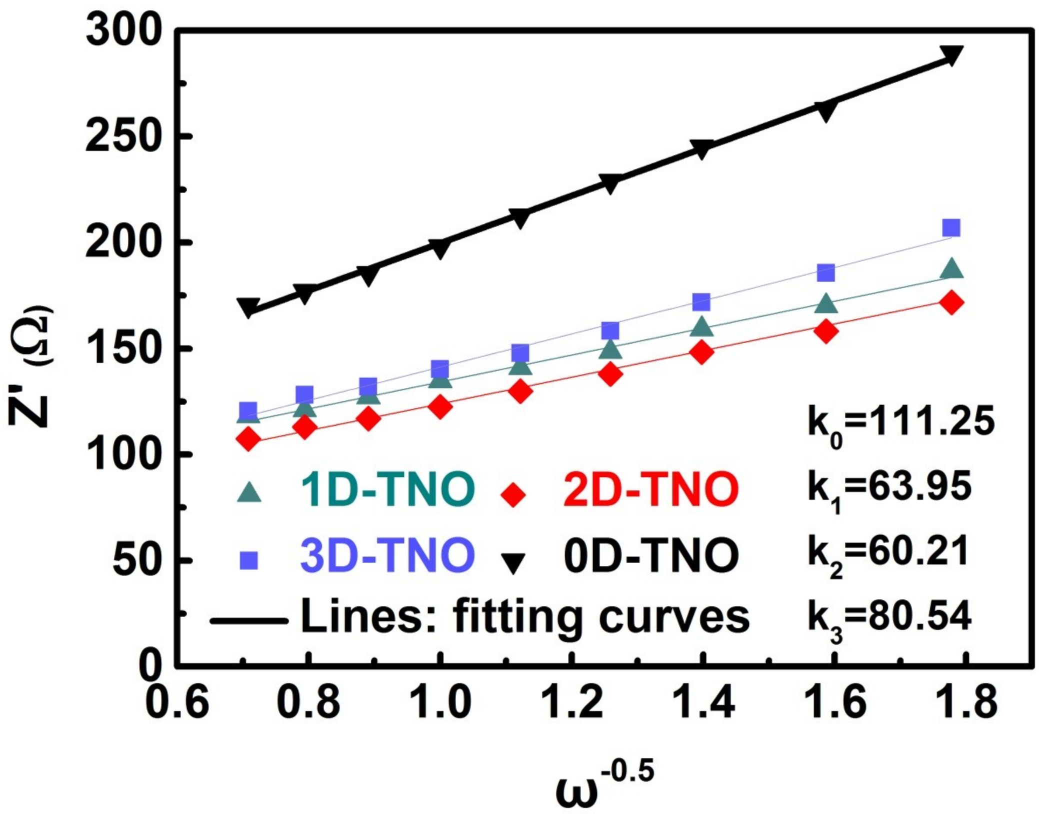

Fig. S5. Z_0–$\omega^{-0.5}$ plots of 0D/1D/2D/3D-TNO samples in the low frequency range.

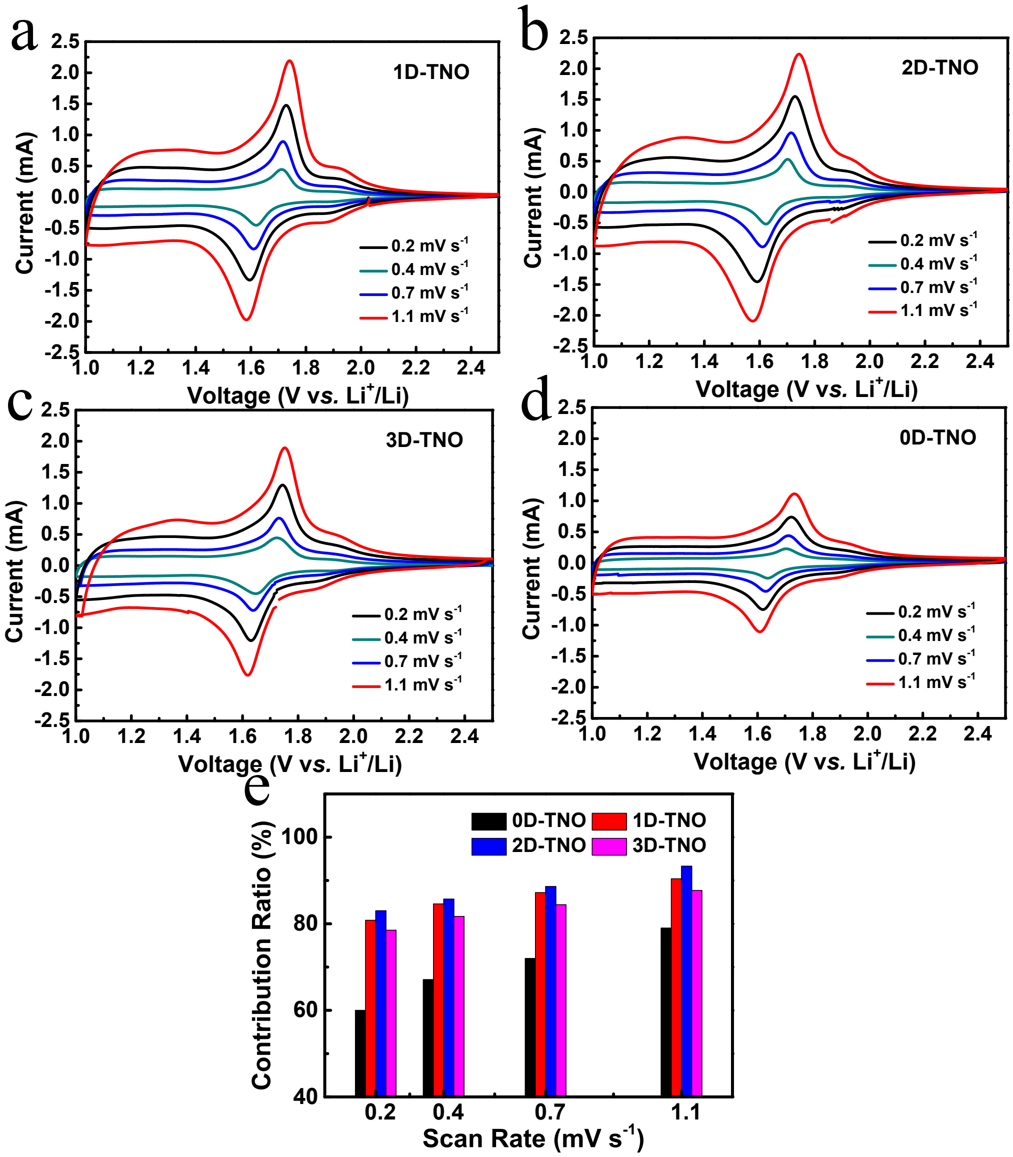

Fig. S6. CV curves of 1D-TNO (a), 2D-TNO (b), 3D-TNO (c) and 0D-TNO (d) electrode at scan rates of 0.2, 0.4, 0.7 and 1.1 mV s^{-1}. (e) Capacitive contribution ratios of the multidimensional TNO electrodes at scan rates of 0.2, 0.4, 0.7 and 1.1 mV s^{-1}, respectively.

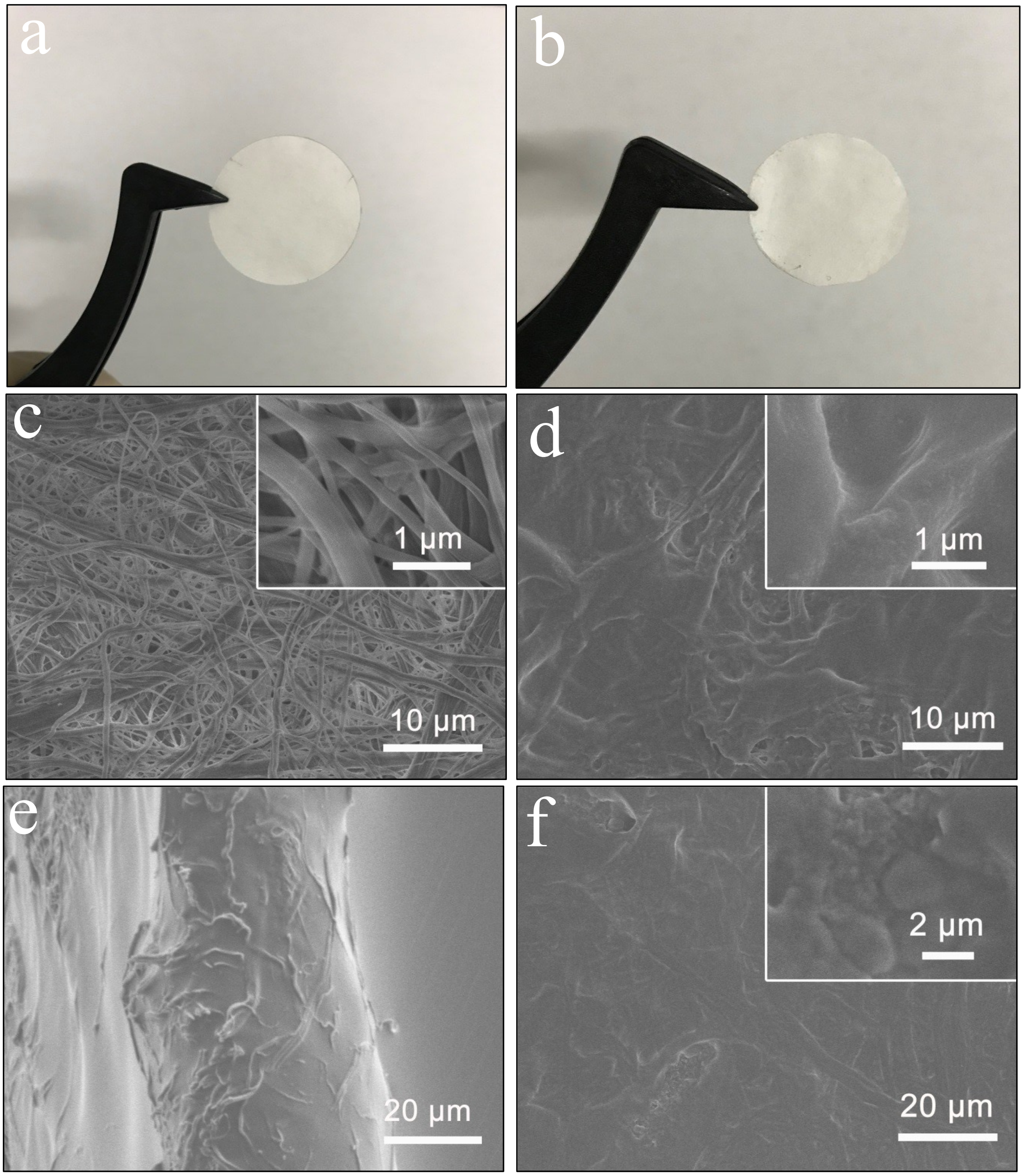

Fig. S7. Optical images of pristine cellulose membrane (a) and CGPE (b); SEM images of pristine cellulose membrane (c) and CGPE (d); (e) Cross-sectional SEM image of CGPE; (f) SEM image of 2D-TNO electrode with GPE.

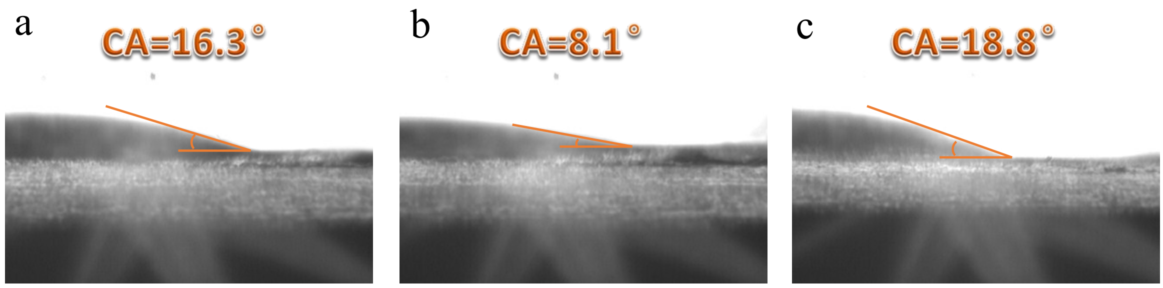

Fig. S8. Contact angle measurements of 1D-TNO (a), 2D-TNO (b), 3D-TNO (c) electrodes

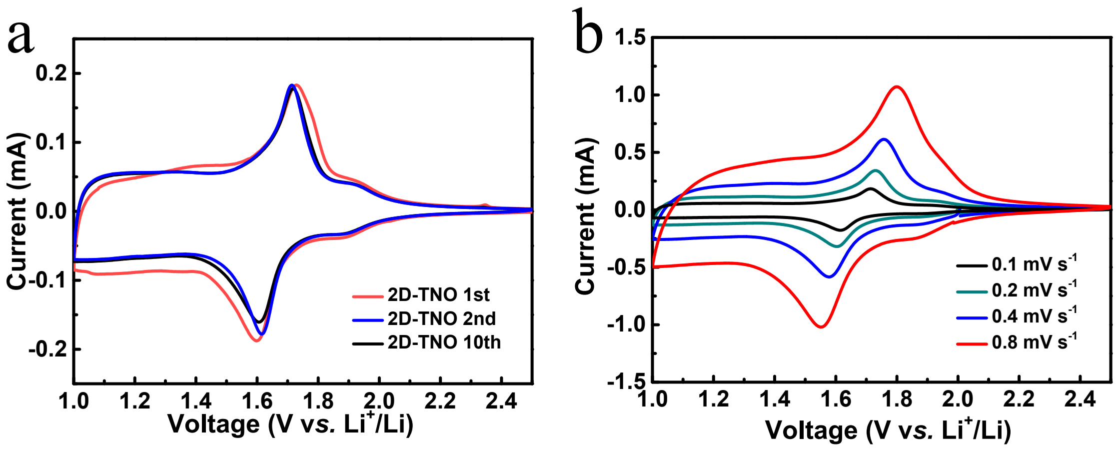

Fig. S9. (a) The 1st, 2nd and 10th CV curves of the half cells based on 2D-TNO electrode at a scan rate of 0.1 mV s^{-1} in solid-state LIBs; (b) CV curves of the half cells based on 2D-TNO electrode at a scan rate of 0.1, 0.2, 0.4 and 0.8 mV s^{-1} in solid-state LIBs

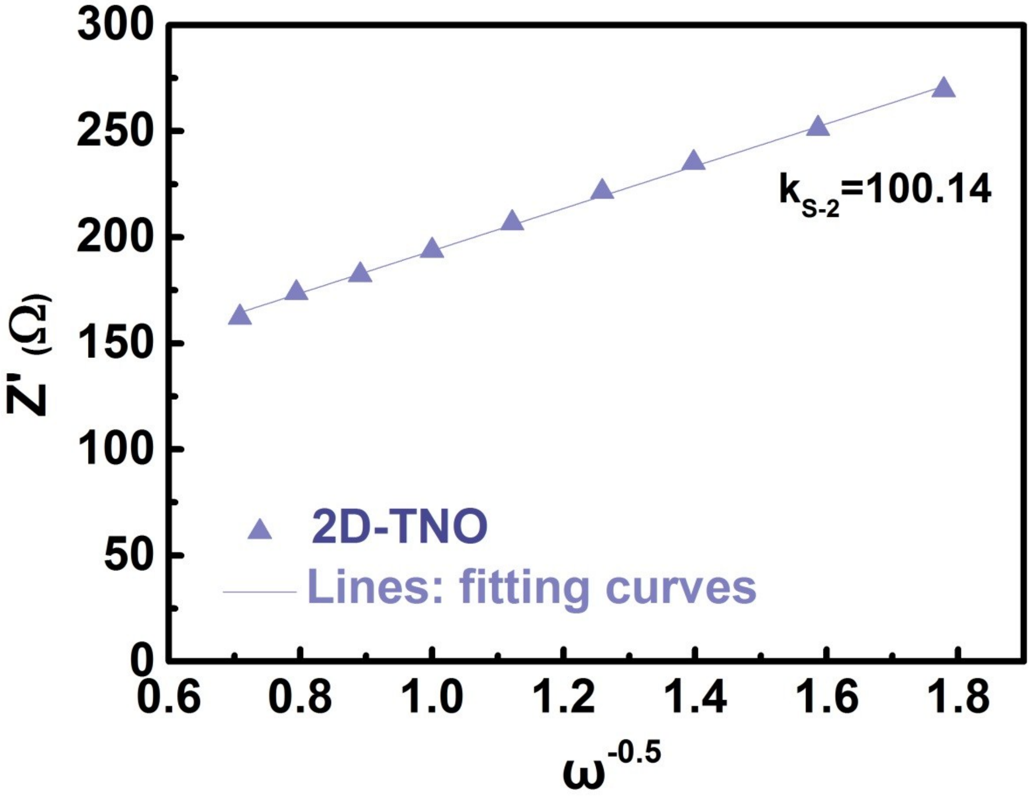

Fig. S10. Z_0–$\omega^{-0.5}$ plot of 2D-TNO electrode in the low frequency range in solid electrolyte

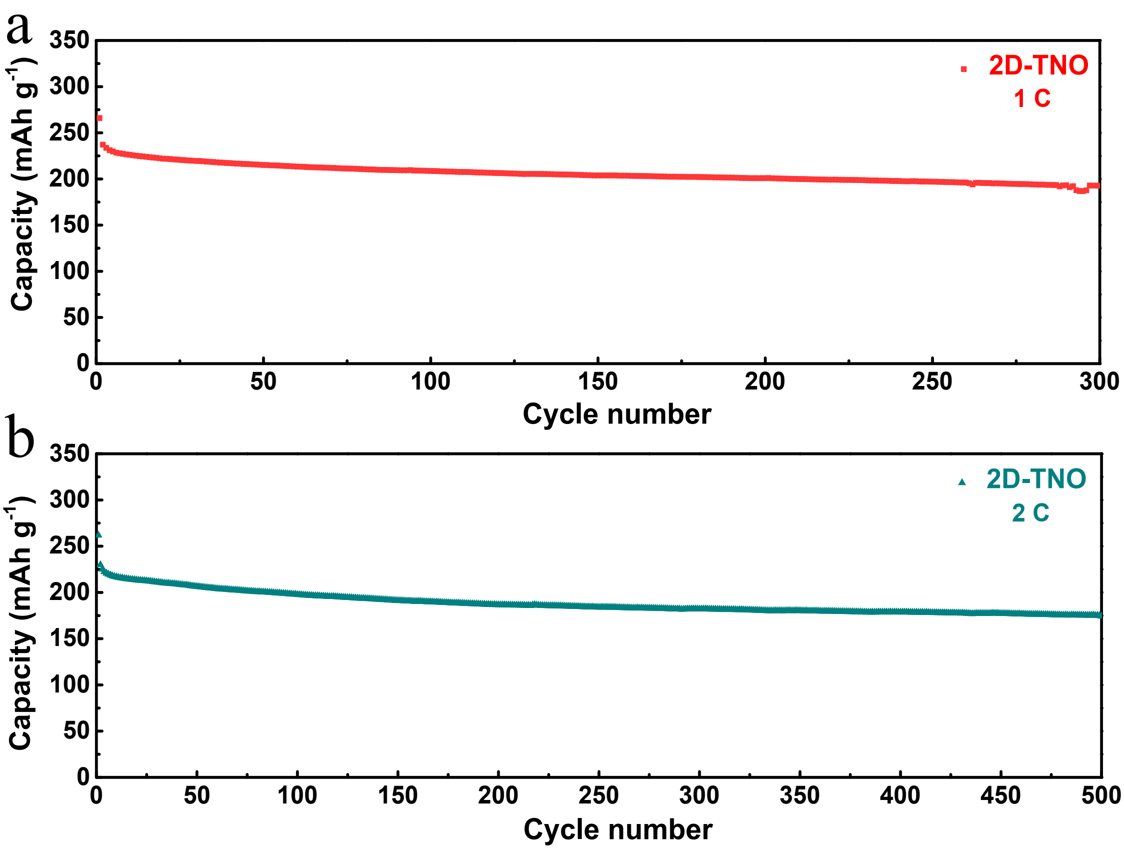

Fig. S11 Cycling performance of 2D-TNO electrode at 1 C (a) and 2 C (b) in solid-state LIBs

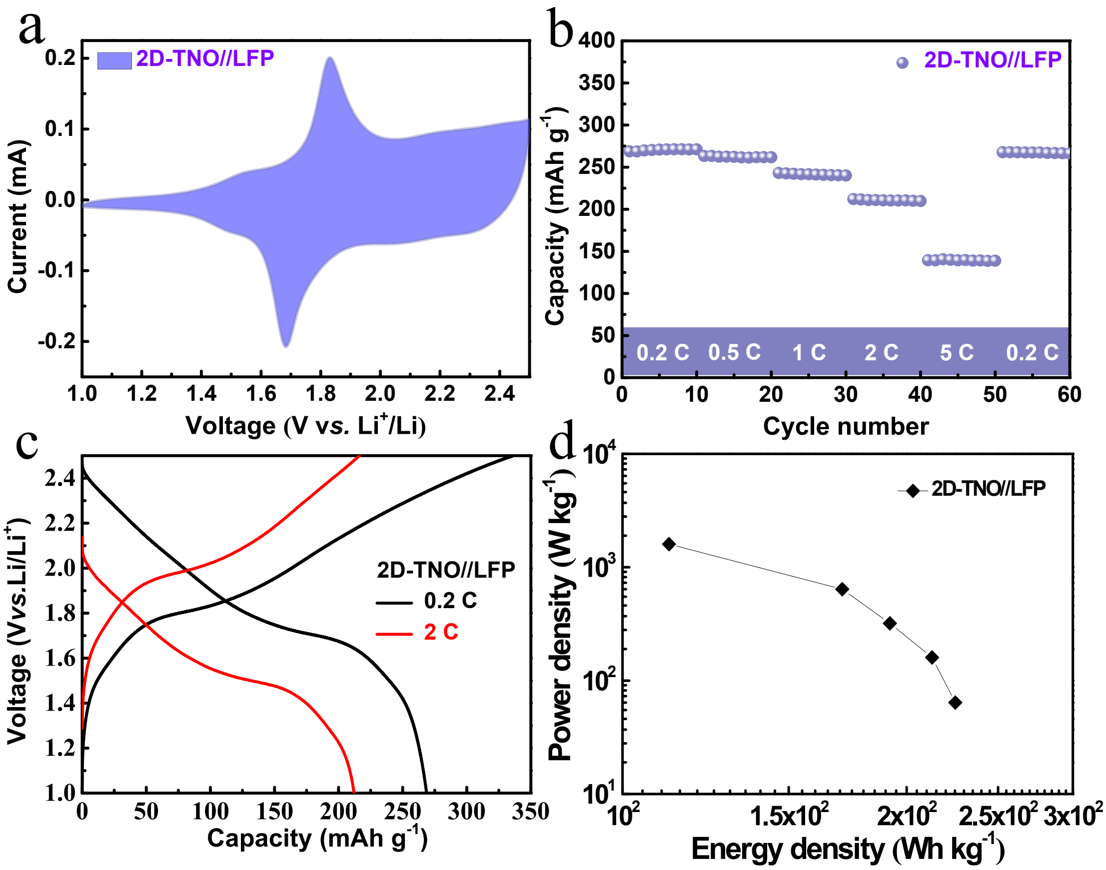

Fig. S12 Electrochemical properties of full cell (2D-TNO//LFP): (a) CV curve at a scan rate of 0.1 mV s^{-1} at the second cycle; (b) Rate performance; (c) Charging/discharging curves at 0.2 C and 2 C; (d) Ragone plot.

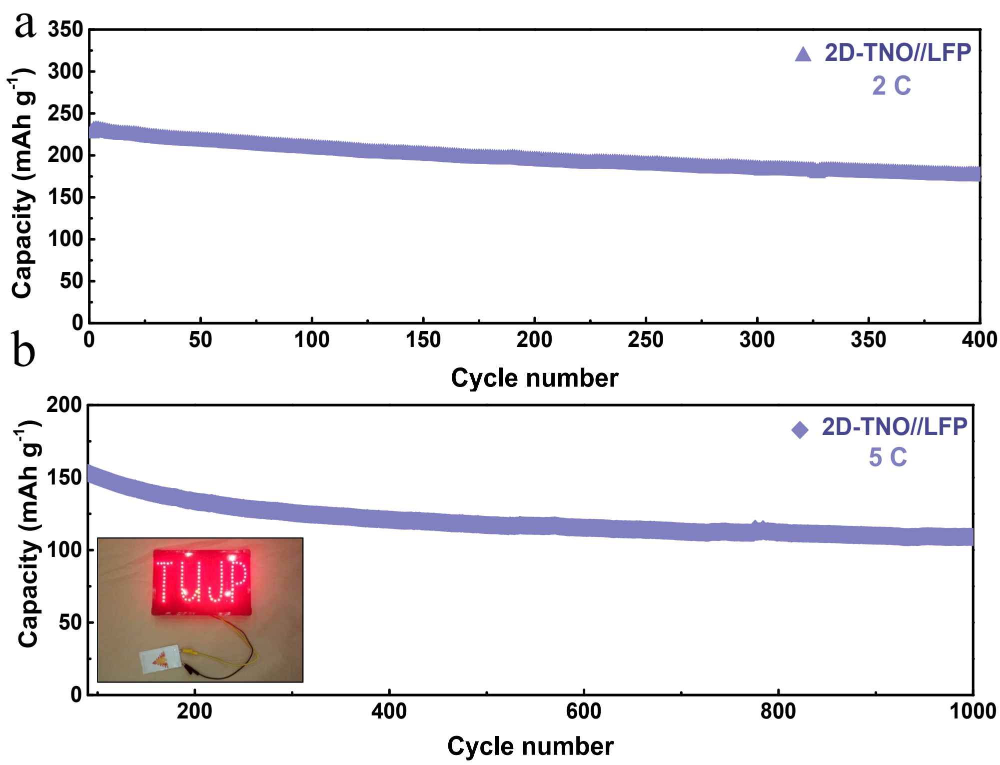

Fig. S13 Cycling performance at 2 C (a) and 5 C (b) (inset: photos of LEDs powered by the assembled full cell) of full cell (2D-TNO//LFP).

Table S1. Simulated EIS results of the 0D/1D/2D/3D-TNO and 2D-TNO (solid state) samples

Electrode	R_s (Ω)	R_{ct} (Ω)	D_{Li}
0D-TNO	5.4	163.5	$7.41x10^{-21}$
1D-TNO	3.8	75.2	$2.24x10^{-20}$
2D-TNO	3.1	62.0	$2.53x10^{-20}$
3D-TNO	4.6	80.6	$1.41x10^{-20}$
2D-TNO (solid state)	5.2	110.1	$9.15x10^{-21}$

Table S2. Rate capacities and cycling performance of multidimensional TNO electrodes

Electrode	Rate performance (mAh g^{-1})							Cycling performance (at 10 C for 1000 cycles, mAh g^{-1})	
	0.5 C	1 C	2 C	5 C	10 C	20 C	40 C	Capacity Initial	Capacity Retention
0D-TNO	204	191	184	171	158	139	97	152	96, 63.2%
1D-TNO	263	246	236	222	207	188	164	204	164, 80.4%
2D-TNO	264	254	244	231	217	197	171	216	177, 81.9%
3D-TNO	260	246	236	218	195	170	144	201	148, 73.6%

Table S3. Capacitive contributions of multidimensional TNO electrodes at different scan rates

Electrode	Capacitive Contribution (%)			
	0.2 mV s^{-1}	0.4 mV s^{-1}	0.7 mV s^{-1}	1.1 mV s^{-1}
0D-TNO	60%	67.1%	72%	79%
1D-TNO	80.8%	84.6%	87.2%	90.4%
2D-TNO	83.0%	85.7%	88.6%	92.3%
3D-TNO	78.5%	81.7%	84.4%	87.7%

Table S4. Electrochemical comparison of other $Ti_2Nb_{10}O_{29}$ based electrodes for lithium ion batteries

Electrodes	**Preparation Method**	**Rate properties (mAh g^{-1})**	**Capacity Initial (mAh g^{-1})**	**Capacity Retention (mAh g^{-1})**	**Rate**	**Ref**
Bulk $Ti_2Nb_{10}O_{29}$	Solid-state reaction	132 (20 C)	212	144 ^{800th}, 68%	10 C	[1]
V-TNO	Solid-state reaction	150 (10 mA cm^{-2})	230	220 ^{30th}, 95%	2 mA cm^{-2}	[2]
$Ti_2Nb_{10}O_{27.1}$	Solid-state	180 (5 C)	198	180 ^{80th}, 91%	5 C	[3]
TNO/rGO	reaction	165 (2 C)	261	182 ^{50th}, 70%	--	[4]
TNO/C	Solid-state reaction Solid-state reaction	145 (30 C)	204	194 ^{100th}, 95%	10 C	[5]
TNO microspheres	Solvothermal method	59 (30 C)	197	185 ^{200th}, 94%	10 C	[6]

Mesoporous $Ti_2Nb_{10}O_{29}$ microspheres	Solvothermal method	171 (30 C)	199	173.5 ^{500th} 86.8%	10 C	[7]
$TiCr_{0.5}Nb_{10.5}O_{29}$/CNTs	Hydrolysis process	206 (20 C)	230	218 ^{100th} 95%	10 C	[8]
$Ti_2Nb_{10}O_{29}$/Ag	Solid state reaction	132 (20 C)	175	142 ^{100th} 81%	10 C	[9]

Table S5. Rate capacities of 2D-TNO electrode in solid-state batteries

Electrode	**Rate performance**						
	0.2 C	0.5 C	1 C	2 C	5 C	10 C	20 C
2D-TNO	244	235	227	216	199	186	159

Table S6. Cycling performance of 2D-TNO electrode in solid-state batteries

2D-TNO Electrode	**Cycling performance**		
	Capacity Initial (mAh g^{-1})	Capacity Retention (mAh g^{-1})	Retention Rate
1 C (300 cycles)	265	192	72.4%
2 C (500 cycles)	261	174	66.7%
5 C (1000 cycles)	238	146	61.3%
10 C (1000 cycles)	235	128	54.5%

Reference

[1] Q. Cheng, J. Liang, Y. Zhu, L. Si, C. Guo, Y. Qian, J. Mater. Chem. A 2014, 2, 17258.

[2] T. Takashima, T. Tojo, R. Inada, Y. Sakurai, J. Power Sources 2015, 276, 113.

[3] C. Lin, S. Yu, H. Zhao, S. Wu, G. Wang, L. Yu, Y. Li, Z. Z. Zhu, J. Li, S. Lin, Sci. Rep. 2015, 5, 17836.

[4] G. Liu, B. Jin, K. Bao, Y. Liu, H. Xie, M. Hu, R. Zhang, Q. Jiang, Int. J. Hydrogen Energy 2017, 42, 22965.

[5] W. L. Wang, B.-Y. Oh, J.-Y. Park, H. Ki, J. Jang, G.-Y. Lee, H.-B. Gu, M.-H. Ham, J. Power Sources 2015, 300, 272.

[6] G. Liu, B. Jin, R. Zhang, K. Bao, H. Xie, J. Guo, M. Wei, Q. Jiang, Int. J. Hydrogen Energy 2016, 41, 14807.

[7] X. Liu, M. Liu, Y. Hu, M. Hu, X. Duan, G. Liu and J. Ma, Ceram. Int., 2019, 45, 3574-3581.

[8] L. Hu, R. Lu, L. Tang, R. Xia, C. Lin, Z. Luo, Y. Chen and J. Li, J. Alloys Compd., 2018, 732, 116-123.

[9] W. Mao, K. Liu, G. Guo, G. Liu, K. Bao, J. Guo, M. Hu, W. Wang, B. Li, K. Zhang and Y. Qian, Electrochim. Acta, 2017, 253, 396-402.